Elastic scattering of two ground-state N atoms*

Zhang Xiao-Niu(张小妞), Shi De-Heng(施德恒)†,
Sun Jin-Feng(孙金锋), and Zhu Zun-Lue(朱遵略)
College of Physics and Information Engineering, Henan Normal University, Xinxiang 453007, *China*

(Received 4 June 2009; revised manuscript received 23 June 2009)

An interaction potential for an $N_2(X^1\Sigma_g^+)$ molecule is constructed by using the highly accurate valence internally contracted multireference configuration interaction method and the largest basis set, aug-cc-pV6Z, in the valence range. The potential is used to investigate the elastic scattering of two N atoms at energies from 1.0×10^{-11} to 1.0×10^{-4} a.u. The derived total elastic cross sections are very large and almost constant at ultralow temperatures, and the shape of total elastic cross section curve is mainly dominated by the *s*-partial wave at very low collision energies. Three shape resonances are found in the total elastic cross sections. Concretely, the first one is very sharp and strong. It results from the *g*-partial-wave contribution and the resonant energy is 3.645×10^{-6} a.u. The second one is contributed by the *h*-partial wave and the resonant energy is 1.752×10^{-5} a.u. This resonance is broadened by those from the *d*- and *f*-partial waves. The third one comes from the $l=6$ partial wave contribution and the resonant energy is 3.522×10^{-5} a.u. This resonance is broadened by those from the *g*- and *h*-partial waves. The $N_2(X^1\Sigma_g^+)$ molecular parameters, which are determined at the current theoretical level, achieve very high accuracy due to the employment of the largest correlation-consistent basis set in the valence range.

Keywords: elastic scattering, total cross section, shape resonance, molecular parameter

PACC: 3520G, 3440

1. Introduction

It is well-known that the nitrogen molecule plays a crucial role in many physical and chemical processes taking place in the atmosphere, aurora and afterglow. However, in spite of its study for many decades, neither an accurate nor a practicable interaction potential for $N_2(X^1\Sigma_g^+)$ has been given in theory. Hence, no investigation into the elastic scattering of two nitrogen atoms in the cold regime can be found, since the elastic collision properties, such as the total and the various partial-wave cross sections, are very sensitive to the details of interaction potential over an extended range of internuclear separations.

One of the main purposes at present is to construct an accurate interaction potential for the $N_2(X^1\Sigma_g^+)$ molecule by using the highly accurate valence internally multireference configuration interaction (MRCI) method[1] and the largest correlation-consistent basis set, aug-cc-pV6Z,[2] in the valence range. With the interaction potential determined at the MRCI/aug-cc-pV6Z level of theory, a total of 59 vibrational states were predicted for the first time through solving the radial Schrödinger equation of nuclear motion by using the Numerov method[3] when the rotational quantum number J is set to be zero. The total and the various partial-wave cross sections are calculated for the elastic scattering of two ground-state N atoms at energies from 1.0×10^{-11} to 1.0×10^{-4} a.u. when they approach each other along the $N_2(X^1\Sigma_g^+)$ potential energy curve (PEC). A comparison between the calculations and the available measurements shows that the present results achieve a very high accuracy due to the employment of the largest correlation-consistent basis set in the valence range. Atomic units are used throughout this paper unless otherwise specified.

2. Interaction potential

We use the MRCI method[1] and the largest correlation-consistent basis set, aug-cc-pV6Z, in the valence range to calculate the harmonic frequency ω_e, equilibrium internuclear distance R_e and PEC of the $N_2(X^1\Sigma_g^+)$ molecule. All the calculations are performed by using the Molpro2008 program package.[4] The R_e and ω_e values determined at this level of theory are listed in Table 1. For convenience of comparison, we also collect the available measurements[5−13] and other theoretical results[14−24] in this Table.

*Project supported by the Program for Science and Technology Innovation Talents in Universities of Henan Province, China (Grant No. 2008HASTIT008), and the National Natural Science Foundation of China (Grant Nos. 60777012 and 10874064).
†Corresponding author. E-mail: scattering@sina.com.cn
© 2010 Chinese Physical Society and IOP Publishing Ltd

Table 1. Spectroscopic parameter comparisons between measurements and other theoretical results for $N_2(X^1\Sigma_g^+)$ at the MRCI/aug-cc-pV6Z level of theory.

source	D_e/eV	R_e/nm	ω_e/cm^{-1}	$\omega_e\chi_e$/cm^{-1}	B_e/cm^{-1}	α_e/cm^{-1}	D_0/eV
this work	9.8555	0.11001	2354.18	14.0975	1.9886	0.01762	9.7101
exp. [5]	9.9008	0.10977	2358.53	14.3006	1.9983	0.01732	9.7550
exp. [6]	–	–	–	–	–	–	9.7543
exp. [7]	9.899	–	–	–	–	–	–
exp. [8]	9.912	–	–	–	–	–	–
exp. [9]	–	0.10976	2358.54	14.3058	1.9982	0.01731	–
exp. [10]	–	–	2358.56	14.3175	1.9982	0.01731	–
exp. [11]	9.9048	0.10977	2358.57	14.324	1.9982	0.01732	9.7594
exp. [12]	9.9048	0.10977	2358.57	14.3244	1.9982	0.01728	9.759
exp. [13]	9.905	–	–	–	–	–	9.7594
theory [14]	–	0.1104	2971	23.55	1.973	0.01198	–
theory [15]	9.34	0.1104	–	–	–	–	–
theory [16]	9.144	0.1103	2349	14.3	–	–	–
theory [17]	8.877	0.1102	2348	–	–	–	–
theory [18]	–	0.110	2372	19.4	–	0.021	–
theory [19]	9.875	0.10974	2366.6	14.1	1.999	0.0171	9.7287
theory [20]	9.038	0.11086	2314	–	–	–	–
theory [21]	–	0.1093	2449	–	–	–	–
theory [22]	–	0.11011	2364.4	13.9142	1.9856	0.01658	–
theory [23]	–	0.10971	2370.9	14.0	–	0.01703	–
theory [24]	9.893	0.11014	2343.1	14.1691	1.9847	0.01718	9.7482

In general, the PEC calculations are made in steps of 0.02 nm over an internuclear distance range from 0.06 to 2.00 nm. Only near the equilibrium position will the step length be 0.005 nm. The PEC is fitted to the Murrell–Sorbie (M–S) function[25] with the least-squares fitting method. Here, the fitted dissociation energy D_e is also collected in Table 1, and the fitting parameters a_i and D_e together with R_e are shown in Table 2 for integrality.

Table 2. APEF parameters for $N_2(X^1\Sigma_g^+)$ at the MRCI/aug-cc-pV6Z level of theory.

D_e/eV	R_e/nm	a_1/nm^{-1}	a_2/nm^{-2}	a_3/nm^{-3}	a_4/nm^{-4}	a_5/nm^{-5}	a_6/nm^{-6}	$\Delta E_{\rm RMSE}$/eV
9.8555	0.11001	57.1222	884.8181	7054.9579	130430.895	–3730567.8	19439966.3	0.00421

To evaluate the fitting quality of the analytic potential energy function (APEF), we calculate the root mean square error ($\Delta E_{\rm RMSE}$) in the fitting process according to the formula given in Ref. [26]. The present $\Delta E_{\rm RMSE}$ is only 0.00421 eV (about 0.0973 Kcal/mol). It is greatly superior to the chemical one (1.0 Kcal/mol).[27] Therefore we conclude that the M–S function is very suitable for reproducing the PEC of this molecule, and the present fitting process is of high quality.

Now, we determine the spectroscopic parameters (B_e, α_e $\omega_e\chi_e$ and D_0) as per the APEF given in Table 2 by the Rydberg–Klein–Rees (RKR) equations.[28] The calculated results are also presented in Table 1.

A number of theoretical spectroscopic investigations[14−24] have been performed on the $N_2(X^1\Sigma_g^+)$ molecule in the past several decades. Of these investigations, the earliest one was made by Fraga and Ransil.[14] Fraga and Ransil carried out $N_2(X^1\Sigma_g^+)$ spectroscopic parameter calculations by using a kind of relatively crude approximation [single configuration method, inner and valence-shell Slater-type Orbital (STO) basis set, and PEC fitted by a third-degree polynomial function]. From Table 1, we find

that the values of ω_e and $\omega_e\chi_e$ greatly deviate from the measurements.[5,9−13] Ermler *et al.*[15] made the calculation of D_e and R_e by the valence CI (VCI) method with a Slater-type Function (STF) basis set, in which five *s*-, four $p\sigma$-, four $p\pi$-, three dσ-, three dπ- and three dδ-type functions centred on each nucleus were contained. Unfortunately, only the values of D_e and R_e were evaluated in their studies. Afterwards, Ermler and Huang[16] computed the values of D_e, R_e, ω_e and $\omega_e\chi_e$ by using the numerical STF VCI method, and Langhoff *et al.*[17] calculated the values of D_e, R_e, ω_e and $\omega_e\chi_e$ by using the complete-active-space self-consistent-field (CASSCF) MRCI method with a very large primitive valence and polarization one-particle Gaussian basis set. Obviously, their D_e results[16,17] greatly deviated from the measurements.[5] Ermler *et al.*[18] evaluated the values of R_e, ω_e, $\omega_e\chi_e$ and α_e by the CI calculations with a double zeta basis set of STF's, which was augmented with a single 3*d*-type polarization function centred on each atom, but the D_e value was not determined in their work. Lately, Werner and Knowles[19] calculated the PEC over an internuclear separation range from 1.6 to 3.5 Bohr by the MRCI method. In their investigations, however, only a small section of PEC was evaluated, and only limited spectroscopic constants were derived. Andersson *et al.*[20] calculated the values of D_e, R_e and ω_e by the second-order perturbation theory based on the CASSCF reference function at various basis sets. Stanton *et al.*[21] computed the values of R_e and ω_e by the equation-of-motion coupled cluster theory with single and double substitutions (EOM-CCSD) at the aug-cc-pVTZ basis set. However, these results[20,21] are inferior to ours when compared with the measurements.[9,11,12] Recently, Li and Paldus[22] calculated the values of R_e, ω_e, $\omega_e\chi_e$, B_e and α_e by using the reduced multireference (RMR) coupled cluster method with singles and doubles (CCSD) and the cc-pVTZ basis set in an eight-dimensional reference space. Pawłwski *et al.*[23] calculated the values of R_e, ω_e, $\omega_e\chi_e$, and α_e by using the MP2 and CCSD(T) methods with a series of correlation-consistent basis sets. However, a very important spectroscopic parameter, D_e, was not computed in their work.[22,23] Very recently, Li and Paldus[24] calculated the spectroscopic parameters and the PEC by using the cc-pVQZ basis set and the RMR CCSD(T) method, which relied on a 56-dimensional reference space. But some molecular parameters, such as the inertial rotation and centrifugal distortion constants, were still not calculated. Thus, the present spectroscopic investigations are the most complete to this day.

From Table 1, one can see that the spectroscopic parameters, R_e and ω_e, which are directly determined by the MRCI/aug-cc-pV6Z calculations, almost perfectly conform with the measurements.[5,9−12] The remaining spectroscopic parameters, D_e, B_e, α_e, $\omega_e\chi_e$ and D_0, which are reproduced from the fitted APEF, are also consistent well with the measurements.[5−13] Calculations show that the deviations between available measurements and the present theoretical results are all within 1.0%. These also prove that the present APEF is accurate.

As is known, a stricter way to compare the *ab initio* results with the measurements is to reproduce the RKR data: the vibrational levels and classical turning points, since only in this way can it be clearly demonstrated whether the present APEF accurately describes this state over a wide range of internuclear separations. In order to attain the vibrational levels and classical turning points, we must solve the radial Schrödinger equation of nuclear motion in the adiabatic approximation,

$$\left[-\frac{\hbar^2}{2\mu}\frac{\mathrm{d}^2}{\mathrm{d}r^2}+\frac{\hbar^2}{2\mu r^2}J(J+1)+V(r)\right]\Psi_{\nu.J}(r) = E_{\nu,J}\Psi_{\nu.J}(r). \quad (1)$$

Here $V(r)$ is the rotationless APEF given in Table 2. r is the internuclear distance between two N atoms. μ is the reduced mass for $N_2(X^1\Sigma_g^+)$. ν and J are the vibrational and the rotational quantum numbers, respectively. $E_{\nu,J}$ and $\Psi_{\nu,J}(r)$ are the eigenvalues and eigenfunctions of the potential $J(J+1)\cdot\hbar^2/2\mu r^2+V(r)$, respectively. The rotational sublevel of a given vibrational level is represented by the following power series:

$$\begin{aligned}E_{\nu,J} = {} & G(\nu)+B_\nu[J(J+1)]-D_\nu[J(J+1)]^2 \\ & +H_\nu[J(J+1)]^3+L_\nu[J(J+1)]^4 \\ & +M_\nu[J(J+1)]^5+N_\nu[J(J+1)]^6 \\ & +O_\nu[J(J+1)]^7, \end{aligned} \quad (2)$$

where $G(\nu)$ is the vibrational level; B_ν is the inertial rotation constant; D_ν, H_ν, L_ν, M_ν, N_ν and O_ν are the centrifugal distortion constants. We employ the Numerov method[3] with automatic step-size selection to solve Eq. (1) numerically, and we obtain a total of 59 vibrational states for $N_2(X^1\Sigma_g^+)$ when the rotational quantum number J is set to equal zero. For each vibrational state, one vibrational level, one inertial rotation constant and 6 centrifugal distortion

constants are determined. Here, to limit the length of this paper, we present only the first 13 vibrational levels, classical turning points, inertial rotation constants and comparisons with the RKR data[10] in Table 3. For the same reason, we present only the first 13 centrifugal distortion constants in Table 4.

Table 3. Comparisons between experimental results and theoretical results of the first 13 vibrational levels, classical turning points and inertial rotation constants for $N_2(X^1\Sigma_g^+)$ when $J = 0$ at the MRCI/aug-cc-pV6Z level of theory.

ν	$G(\nu)/cm^{-1}$	R_{min}/nm	R_{max}/nm	B_ν/cm^{-1}
0	1178.255 (1175.773)	0.10578 (0.105491)	0.11474 (0.114551)	1.982791 (1.989574)
1	3510.396 (3505.685)	0.10294 (0.102644)	0.11857(0.118417)	1.964051 (1.972203)
2	5815.300 (5806.927)	0.10108 (0.100812)	0.12143(0.121280)	1.947556 (1.95477)
3	8085.922 (8079.47)	0.09963 (0.099396)	0.12389 (0.123741)	1.934194 (1.93728)
4	10332.121 (10320.28)	0.09840 (0.098212)	0.12614 (0.125974)	1.918570 (1.91973)
5	12541.660 (12538.31)	0.09733 (0.097211)	0.12822 (0.128057)	1.900693 (1.90211)
6	14725.207 (14724.54)	0.09636 (0.096319)	0.13021 (0.130036)	1.885969 (1.88443)
7	16883.336 (16881.89)	0.09547 (0.095520)	0.13212 (0.131937)	1.871710 (1.86669)
8	18996.520 (19010.34)	0.09465 (0.094794)	0.13396 (0.133780)	1.857930 (1.84888)
9	21105.137 (21109.8)	0.09387 (0.094129)	0.13577 (0.135578)	1.836450 (1.8310)
10	23169.462 (23180.2)	0.09314 (0.093514)	0.13573 (0.137341)	1.819301 (1.8131)
11	25213.666 (25221.6)	0.09243 (0.092943)	0.13927 (0.139077)	1.798172 (1.7951)
12	27205.808 (27233.7)	0.09175 (0.092410)	0.14097 (0.140793)	1.780175 (1.7770)
13	29198.834 (29216.7)	0.09108 (0.091910)	0.14267 (0.142493)	1.773926 (1.7589)

Data in parentheses are the RKR data cited from Ref. [10].

From Table 3, we can clearly see that the present results are in excellent agreement with the RKR data. For the vibrational levels, the classical turning points or the inertial rotation constants, their values deviate from the corresponding RKR data all within 1.0%. Therefore, we further conclude that the values of APEF presented in Table 2 are reliable.

Table 4. The first 13 centrifugal distortion constants for $N_2(X^1\Sigma_g^+)$ when $J = 0$ at the MRCI/ aug-cc-pV6Z level of theory.

ν	$D_\nu(\times10^{6})/cm^{-1}$	$H_\nu(\times10^{12})/cm^{-1}$	$L_\nu(\times10^{-16})/cm^{-1}$	$M_\nu(\times10^{21})/cm^{-1}$	$N_\nu(\times10^{-26})/cm^{-1}$	$O_\nu(\times10^{31})/cm^{-1}$
0	5.567470	5.029184	–1.257961	1.294205	–1.564552	2.544261
1	5.686308	7.480760	–1.575903	1.914050	–2.863950	4.970073
2	5.810308	10.22444	–2.005714	2.796617	–4.909636	9.401457
3	5.941471	13.31874	–2.578673	4.068855	–8.144063	17.37279
4	6.082067	16.84495	–3.337883	5.919865	–13.30077	31.65975
5	6.234705	20.91462	–4.344159	8.637355	–21.61195	57.35043
6	6.402424	25.68039	–5.685086	12.66826	–35.17122	103.7759
7	6.588848	31.35214	–7.489047	18.71732	–57.52731	187.4774
8	6.798388	38.22077	–9.946337	27.89314	–94.45345	334.4163
9	7.036546	46.69192	–13.33742	41.86336	–154.0985	570.7630
10	7.310299	57.32708	–18.05675	62.77945	–243.0104	861.8113
11	7.628548	70.87018	–24.58047	9.209897	–346.6646	879.6785
12	8.002330	88.18024	–33.21544	125.8358	–365.3589	–668.3603
13	8.443979	109.8490	–43.22235	140.7288	48.67228	–7480.213

Unfortunately, both experimentally and theoretically, little information about the centrifugal distortion constants for $N_2(X^1\Sigma_g^+)$ can be found, to our knowledge. But according to the high-quality fitting process of the APEF, the excellent agreement between the present spectroscopic parameters and the measurements[5−13] and the good accordance between the present values listed in Table 3 and the RKR data,[10] we have reason to believe that the results collected in Table 4 are all accurate, thereby proving that the present APEF accurately describes the $X^1\Sigma_g^+$ state of the N_2 molecule.

3. Total and partial-wave elastic cross sections

Now we use the APEF obtained in this paper to calculate the total and the various partial-wave cross sections of collisions between two nitrogen atoms. Therefore we must obtain the radial solution u_l of the l-th partial-wave equation, i.e. we must solve the radial Schrödinger equation[29]

$$\frac{\mathrm{d}^2u_l}{\mathrm{d}r^2}+\left[k^2-\frac{2\mu V(r)}{\hbar^2}-\frac{l(l+1)}{r^2}\right]u_l(r)=0. \quad (3)$$

Here, $V(r)$ is the APEF given in Table 2. μ is the reduced mass of the colliding system, two N atoms. k is the wave number, which is determined from the energy E of relative motion through $k^2=2\mu E/\hbar^2$. With the obtained u_l, the scattering phase shift δ_l of the l-th partial wave can be derived from

$$\tan\delta_l=\frac{-2\mu}{\hbar^2k}\int_0^\infty j_l(kr)V(r)u_l(r)\mathrm{d}r, \quad (4)$$

where l is equal to 0, 1, 2, ... The elastic cross section of the l-th partial wave, $\sigma_l(E)$, is determined by

$$\sigma_l(E)=\frac{4\pi}{k^2}\cdot(2l+1)\sin^2\delta_l. \quad (5)$$

Then, the total elastic cross section, $\sigma_T(E)$, can be calculated by

$$\sigma_{\mathrm{T}}(E)=\sum_{l=0}^{\infty}\sigma_l(E)=\frac{4\pi}{k^2}\sum_{l=0}^{\infty}(2l+1)\sin^2\delta_l. \quad (6)$$

Using the APEF tabulated in Table 2, equation (3) can be numerically solved by the Numerov method[3] with automatic step-size selection. The partial-wave phase shift δ_l of the elastic collisions between two N atoms at low temperatures is evaluated according to expression (4) when two N atoms approach each other along the $N_2(X^1\Sigma_g^+)$ PEC. Various elastic partial-wave cross sections and the total elastic cross sections are computed as per expressions (5) and (6) at impact energies from 1.0×10^{-11} to 1.0×10^{-4} a.u. The collision energy dependence of the total elastic cross section at low and ultralow temperatures is depicted in Fig. 1, and the collision energy dependences of elastic cross sections for various partial waves are presented in Figs. 2–6, respectively.

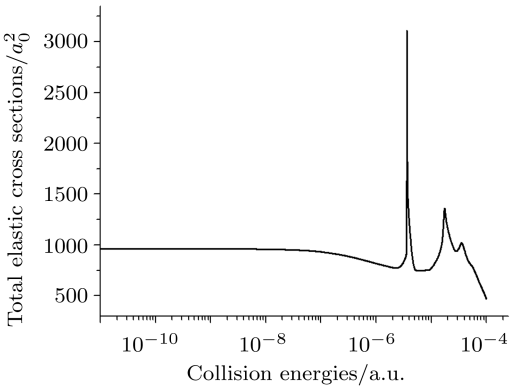


Fig. 1. Total elastic cross sections versus collision energies for scattering along the N_2 ground-state PEC.

As shown in Fig. 1, the total cross sections of elastic scattering of two N atoms in the ground state are very large and almost constant at ultralow temperatures. From Figs. 2–6, we can see that the s-wave cross sections are significant but the remaining partial-wave cross sections are very small when the collision energy is below 10^{-6} a.u. Especially when the energy is lower than 10^{-7} a.u., only the s wave has contributions to the total cross sections. Therefore, the total elastic cross sections are dominated by the s-wave scattering over this impact energy regime. With impact energy increasing, the s-wave cross sections tend to decrease, but the decrease is quickly overcome by the higher partial-wave contributions. It can be clearly seen in Fig. 1 and Figs. 3–6. Particularly when the energy is higher than 10^{-6} a.u., the significance of the higher partial waves greatly becomes prominent. Thus, as demonstrated in Fig. 1, some resonant peaks occur by the addition of higher partial waves.

Three resonant structures can be found in Fig. 1. At very low temperatures, with collision energy increasing, the first shape resonance appears. Obviously, this resonance is rather sharp and strong. Accurate calculations indicate that this peak results from the g-partial-wave shape resonance and the resonant energy is 3.645×10^{-6} a.u. Subsequently, the second

peak arrives. This peak is also strong but rather weak when compared with the first one. Accurate calculations demonstrate that it mainly results from the h-wave contributions and the resonant position in the total elastic cross sections is at energy of 1.752×10^{-5} a.u. The last one is the weakest among the three peaks. Accurate calculations point out that it comes mainly from the $l = 6$ wave contributions and the resonant energy is 3.522×10^{-5} a.u.

Figure 2 shows that two weak resonant peaks exist in the s partial-wave cross sections and the resonant energies are 2.257×10^{-5} and 7.552×10^{-5} a.u., respectively. Because these peaks are so weak that they are drowned in the strong total elastic cross sections.

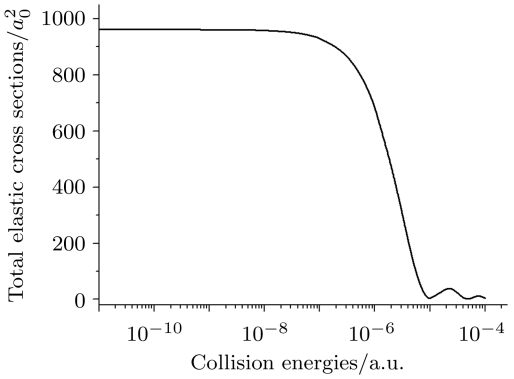


Fig. 2. s partial-wave cross sections versus collision energies for scattering along the N_2 ground-state PEC.

Figure 3 presents the collision energy dependences of elastic cross sections for p-, d- and f-partial waves. As shown in Fig. 3, one can instantly see that there appear rich structures in these partial waves. For example, two resonances are found in the p-partial wave and the resonant energies are 4.990×10^{-6} and 4.115×10^{-5} a.u., respectively. Two peaks exist in the d-partial wave and the resonant energies are 1.234×10^{-5} and 6.400×10^{-5} a.u., respectively. One structure emerges in the f-partial wave and the resonant energy is 2.150×10^{-5} a.u. Compared with the resonances of the s partial wave, these resonances are so weak that they all pass into oblivion by the strong s partial wave cross sections. The scenarios are the same as those in the $l = 7$ and 8 partial-wave cross sections.

There appears a very sharp resonance in Fig. 4. Accurate calculations point out that its resonant energy is 3.645×10^{-6} a.u., which is strictly consistent with that in the first peak demonstrated in Fig. 1. Accurate examination indicates no resonance existing around the energy of 3.645×10^{-6} a.u. except for the g-partial wave. Therefore, the strong and sharp peak in the total elastic cross sections is contributed only by the g-partial wave.

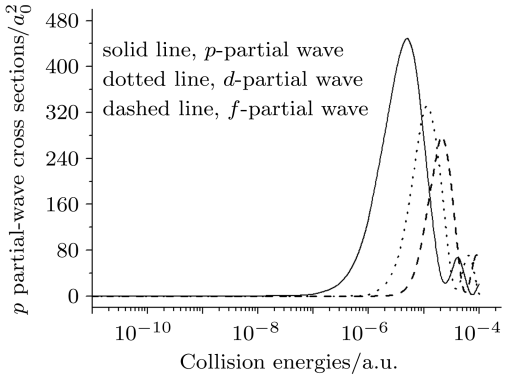


Fig. 3. p, d and f partial-wave cross sections versus collision energies for scattering along the N_2 ground-state PEC.

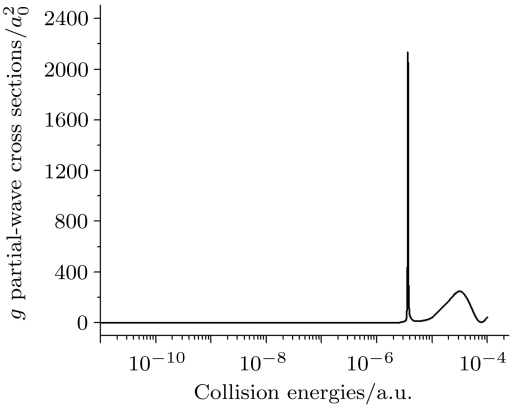


Fig. 4. g partial-wave cross sections versus collision energies for scattering in the N_2 ground state.

Figure 5 presents two shape resonances in the h-partial wave. The resonant energy of the strong one is 1.752×10^{-5} a.u., which is consistent with that in the

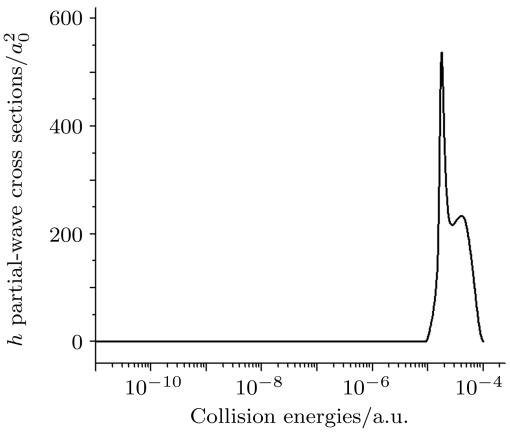


Fig. 5. h partial-wave cross sections versus collision energies for scattering along the N_2 ground-state PEC.

second peak depicted in Fig. 1. It is easy to find that the second peak in Fig. 1 is not sharp. The reason is that this peak is contributed by different partial waves. If we carefully examine the resonances in Fig. 3, we can find two shape resonances, whose resonant energies are both around 1.752×10^{-5} a.u., or rather, one comes from the p-partial wave, whose resonant energy is 1.234×10^{-5} a.u. The other comes from the f-partial wave, whose resonant energy is 2.150×10^{-5} a.u. It is the two resonances that broaden the second peak in the total elastic cross sections.

Only one resonance can be found in the $l = 6$ partial-wave cross sections in Fig. 6. Investigations show that the resonant energy of this peak is 3.522×10^{-5} a.u., which is completely consistent with the third resonance in the total elastic cross sections. It is not difficult to find that the resonant peak in Fig. 6 is very sharp. But in contrast with this, the third peak in Fig. 1 is very wide. In similarity with the second peak in Fig. 1, the third peak is also contributed by different partial waves. If we carefully examine the resonances in Figs. 4 and 5, we can easily find that two resonances exist around the energy, 3.522×10^{-5} a.u. Specifically one appears in Fig. 4, and its resonant energy is 3.192×10^{-5} a.u. The other occurs in Fig. 5, and its resonant energy is 4.030×10^{-5} a.u. It is these peaks that broaden the third resonance in Fig. 1.

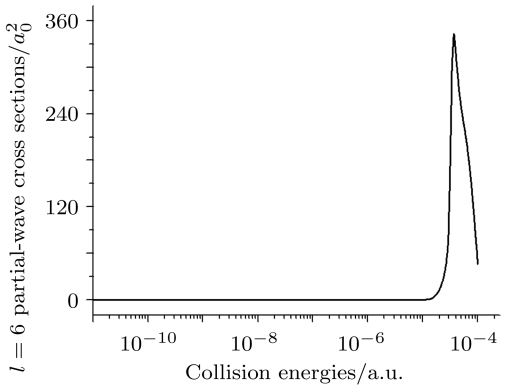


Fig. 6. $l = 6$ partial-wave cross sections versus collision energies for scattering along the N_2 ground-state PEC.

Two resonances occur in the $l = 7$ and 8 partial-wave cross sections. One appears in the $l = 7$ wave and the resonant energy is 6.190×10^{-5} a.u., and the other is found in the $l = 8$ wave and the resonant energy is 9.110×10^{-5} a.u. Due to too much weakness, these resonances are completely drowned in the strong total elastic cross sections. When the partial-wave number is higher than 8, no resonances exist. Also, when the partial-wave number is higher than 10, their contributions to the total elastic cross sections can be neglected.

4. Conclusions

The equilibrium internuclear separation, the harmonic frequency and the PEC of the $N_2(X^1\Sigma_g^+)$ molecule are investigated by using the MRCI theory and the largest correlation-consistent basis set, aug-cc-pV6Z, in the valence range. The APEF obtained over the internuclear distance range from 0.06 to 2.00 nm is used to determine the spectroscopic parameters, D_e, $\omega_e\chi_e$, α_e, B_e and D_0. With the potential derived at the MRCI/aug-cc-pV6Z level of theory, a total of 59 vibrational states are predicted by numerically solving the radial Schrödinger equation of nuclear motion with the Numerov method. For each vibrational state, the vibrational level, the classical turning points, the inertial rotation constants and the centrifugal distortion constants are also calculated when $J = 0$. The total and various elastic cross sections of two N collisions are investigated for the first time when they approach each other along the $N_2(X^1\Sigma_g^+)$ PEC. Three peaks are found in the total elastic cross sections, and their resonant energies are 3.645×10^{-6}, 1.752×10^{-5} and 3.522×10^{-5} a.u., respectively. Concretely, the first peak results from the g-wave contributions; the second peak is contributed mainly by the h wave and broadened by the resonances from the d and f waves; the third peak comes mainly from the $l = 6$ wave contributions and it is broadened by the resonances from the g and h waves. Analyses show that the shapes of the total elastic cross sections are mainly dominated by the s-partial wave at very low temperatures.

References

[1] Werner H J and Knowles P J 1988 *J. Chem. Phys.* **89** 5803

[2] Peterson K A, Kendall R A and Dunning T H 1993 *J. Chem. Phys.* **99** 1930

[3] González J L M Q and Thompson D 1997 *Comput. Phys.* **11** 514

[4] Werner H J, Knowles P J, Lindh R, Manby F R, Schütz M, Celani P, Korona T, Mitrushenkov A, Rauhut G, Adler

T B, Amos R D, Bernhardsson A, Berning A, Cooper D L, Deegan M J O, Dobbyn A J, Eckert F, Goll E, Hampel C, Hetzer G, Hrenar T, Knizia G, Köppl C, Liu Y, Lloyd A W, Mata R A, May A J, McNicholas S J, Meyer W, Mura M E, Nicklass A, Palmieri P, Pflüger K, Pitzer R, Reiher M, Schumann U, Stoll H, Stone A J, Tarroni R, Thorsteinsson T, Wang M and Wolf A 2008 *MOLPRO* (version 2008.1) *A Package of ab initio Programs*

[5] Le Roy R J, Huang Y Y and Jary C 2006 *J. Chem. Phys.* **125** 164310

[6] Tang X N, Hou Y, Ng C Y and Ruscic B 2005 *J. Chem. Phys.* **123** 074330

[7] Roncin J Y, Launay F, Bredohl H and Dubois I 1999 *J. Mol. Spectrosc.* **194** 243

[8] Chase M W 1998 *NIST-JANAF Tables, J. Phys. Chem. Ref. Data Monographs*, (Vol.9, 4th edition) (New York: American Institute of Physics)

[9] Orlov M L, Ogilvie J F and Nibler J W 1997 *J. Mol. Spectrosc.* **185** 128

[10] Edwards S, Roncin J Y, Launay F and Rostas F 1993 *J. Mol. Spectrosc.* **162** 257

[11] Huber K P and Herzberg G 1979 *Molecular Spectra and Molecular Structure* (Vol.4). *Constants of Diatomic Molecules* (New York: Van Nostrand Reinhold Company) p420

[12] Lofthus A and Krupenie P H 1977 *J. Phys. Chem. Ref. Data* **6** 113

[13] Buttenbender G and Herzberg G 1934 *Ann. Phys.* (Leipzig) **21** 57

[14] Fraga S and Ransil B J 1961 *J. Chem. Phys.* **35** 669

[15] Ermler W C, McLean A D and Mulliken R S 1982 *J. Phys. Chem.* **86** 1305

[16] Ermler W C and Huang C W 1985 *Chem. Phys. Lett.* **120** 159

[17] Langhoff S R, Bauschlicher C W and Taylor P R 1987 *Chem. Phys. Lett.* **135** 543

[18] Ermler W C, Clark J P and Mulliken R S 1987 *J. Chem. Phys.* **86** 370

[19] Werner H J and Knowles P J 1991 *J. Chem. Phys.* **94** 1264

[20] Andersson K, Malmqvist P Å and Roos B O 1992 *J. Chem. Phys.* **96** 1218

[21] Stanton J F, Gauss J, Ishikawa N and Head-Gordon M 1995 *J. Chem. Phys.* **103** 4160

[22] Li X Z and Paldus J 2000 *J. Chem. Phys.* **113** 9966

[23] Pawłwski F, Halkier A, Jørgensen P, Bak K L, Helgaker T and Klopper W 2003 *J. Chem. Phys.* **118** 2539

[24] Li X Z and Paldus J 2008 *J. Chem. Phys.* **129** 054104

[25] Shi D H, Zhang J P, Sun J F, Liu Y F and Zhu Z L 2008 *Acta Phys. Sin.* **58** 2369 (in Chinese)

[26] Shi D H, Zhang J P, Liu Y F, Sun J F and Yu B H 2008 *J. Mol. Struct.* (*Theochem*) **861** 74

[27] Aguado A and Paniagua M 1992 *J. Chem. Phys.* **96** 1265

[28] Shi D H, Zhang J P, Liu Y F, Sun J F and Zhu Z L 2009 *Int. J. Quant. Chem.* **109** 1159

[29] Shi D H, Zhang J P, Sun J F and Zhu Z L 2009 *Chin. Phys.* B **18** 2250